Available online at www.sciencedirect.com
ScienceDirect
Composites: Part A 39 (2008) 786–795
composites
Part A: applied science and manufacturing
www.elsevier.com/locate/compositesa

Reinforcing an aluminum/GFRP co-cured single lap joint using inter-adherend fiber

Ryosuke Matsuzaki [a,*], Motoko Shibata [b,1], Akira Todoroki [b,1]

[a] Department of Mechanical Sciences and Engineering, Tokyo Institute of Technology 2-12-1-I1-66, O-okayama Meguro-ku, Tokyo 152-8552, Japan
[b] Department of Mechanical Sciences and Engineering, Tokyo Institute of Technology 2-12-1-I1-58, O-okayama Meguro-ku, Tokyo 152-8552, Japan

Received 5 October 2007; received in revised form 28 January 2008; accepted 2 February 2008

Abstract

Methods to increase the strength of co-cured joints are highly sought after for metal/composite hybrid structures. The present study proposes a reinforcing method for aluminum/glass fiber-reinforced polymer co-cured composites using inter-adherend (IA) fiber that penetrates into the composite and holes in the metal adherend. The IA fiber performs as a bridge and suppresses crack propagation in the lap joints. Static and fatigue tensile tests were performed, and the displacement to failure and ultimate static strength were found to be significantly increased using the IA fiber without a decrease in the fatigue performance. The optimal tension force to the IA fiber realizes higher static tensile strength with lower scatter.

Keywords: A. Glass fibers; B. Strength; E. Joints/joining; Co-cure

1. Introduction

Fiber reinforced plastic (FRP) composites are superior to metals in terms of specific strength and stiffness, nevertheless metals are still important due to their high reliability in actual structures. Hence, structures are usually made of a hybrid of composites and metals. To reduce manufacturing time and the cost of joining metals and composites, co-curing has been developed [1–7]. The co-cured joint uses the excess resin of FRP as an adhesive, so that the adhesive and FRP adherend are united. Thus, curing and joining processes for composite structures can be achieved simultaneously. Although the reduction in labor for the additional curing process is favorable, a dramatic increase in joining strength compared with conventional adhesively bonded joints cannot be expected. Therefore, methods to increase the strength of co-cured joints are highly sought after.

To reinforce a co-cured composite/composite lap joint, through-thickness reinforcements such as stitching and z-pinning were developed. Stitching is a technique that requires sewing a continuous high-strength reinforcing thread through multiple uncured prepreg laminas before the impregnation phase. Many investigators [8–15] have shown that through-thickness stitching for laminated composites improves Mode I and II fracture toughness. The concept of stitching has been applied to the lap joints between composites. Tong et al. [16,17] conducted an angled stitching and demonstrated that stitched joints were over 20% stronger and had 25% greater strain-to-failure than their unstitched counterparts. Aymerich et al. [18,19] applied the stitching to graphite/epoxy bonded joints and showed that it reduced G_I and prolonged the duration of the crack propagation phase under fatigue loading.

Z-pins, i.e. small diameter cylindrical rods embedded in the composite material and oriented perpendicular to the layer interface, were developed to enhance fracture and fatigue resistances of co-cured joints between composites

* Corresponding author. Tel./fax: +81 3 5734 3184.
E-mail addresses: rmatsuza@ginza.mes.titech.ac.jp (R. Matsuzaki), mshibata@ginza.mes.titech.ac.jp (M. Shibata), atodorok@ginza.mes.titech.ac.jp (A. Todoroki).
[1] Tel./fax: +81 3 5734 3178.

1359-835X/$ - see front matter © 2008 Elsevier Ltd. All rights reserved.
doi:10.1016/j.compositesa.2008.02.002

[20,21]. Chang et al. [22,23] showed z-pinning was effective in increasing the ultimate strength and fatigue life. However, the conventional through-thickness reinforcements used the penetrability of uncured prepreg or dry cloth preform; it is impossible to apply these through-thickness reinforcements to metallic materials, where the fibers cannot be sewn due to the high hardness of metals.

As for reinforcing metal/composite co-cured lap joints, Melograna et al. proposed perforation [24] and tongue-and-groove [25] methods; Matsuzaki et al. [26] proposed a dimple method. Although these methods allow an increase in the strength of the metal/composite co-cured lap joints, the perforation and tongue-and-groove need high-precision processing using a water-jet cutter; the dimple method requires the appropriate rod tools for the dimple treatment. Fabrication requiring special skills becomes an obstacle for low-cost manufacturing.

In previous studies, to simplify the manufacturing process for reinforcing metal/composite joints, we proposed a bolted/co-cured hybrid joining method. The method combines co-cured adhesive joints and bolted joints without damaging reinforcing fibers of composite adherends [27]. The proposed joint allows for high stable strength in static and fatigue loading, and is easily manufactured. However, the method uses several bolts to enhance the fracture toughness, and it is problematic in increasing the weight of structures especially for recent weight saving designed structures. Thus, a lightweight and easy-to-fabricate joint reinforcing method is required for metal/composite co-cured joints.

The present paper proposes a novel reinforcing method for metal/composite co-cured joints using inter-adherend (IA) fibers. In this method, two small holes are fabricated in the metallic adherend, and high strength and through-thickness fibers named IA fibers penetrate through holes in the metal adherend and uncured prepreg. The IA fibers may enhance the crack propagation resistance, and increase the strength of metal/composite co-cured joints. Experimental testing of the static and fatigue tensile lap-shear strength is performed using specimens of inter-adherend-fiber (IAF) joints between aluminum alloy A5052-F and plain-woven glass epoxy composites. For comparison, non-IAF co-cured joints are also tested. The effect of the IA fiber tension force on the joint strength is also investigated.

2. Inter-adherend-fiber joint

A schematic illustration of an IAF joint is shown in Fig. 1. A high strength through-thickness fiber named Inter-Adherend fiber penetrates into prepared holes drilled in the metal adherend and a composite prepreg. The IA fiber acts as a bridge when a crack occurs, which reduces the driving force of the crack propagation at the crack tip, and suppresses or delays the propagation between the adherends.

In single lap joints under tensile loading, shear and peeling stresses occur and are at a maximum at the edge of the over-lap area due to the presence of the bending moment. As for the aluminum/glass fiber-reinforced polymer (GFRP) lap joints, a crack occurs at the aluminum adherend edge first because of a higher stiffness of the aluminum adherend than of the GFRP [27]. As a consequence, IA fibers are employed at the edge of the aluminum adherend to improve the crack propagation resistance.

The penetrating process of the IA fiber into the composite prepreg uses the space between glass fiber bundles of woven GFRP fabric by manual sewing as shown in Fig. 2; thereby, it neither breaks the glass fibers nor disarranges the fiber alignments. This benefit may prevent a decrease in fatigue strength, which is seen in stitching that uses a sewing machine. Since it uses holes in the metallic adherend, the IAF method can be applied not only to metallic materials but to any hard material such as ceramics and plastics.

3. Experimental procedures

3.1. Specimen preparation

The specimens of IAF joints are single-lap designs based on Japanese Industrial Standards (JIS) K6850: testing methods for tensile lap-shear strength of adhesive bonds. A schematic configuration showing the dimensions of the

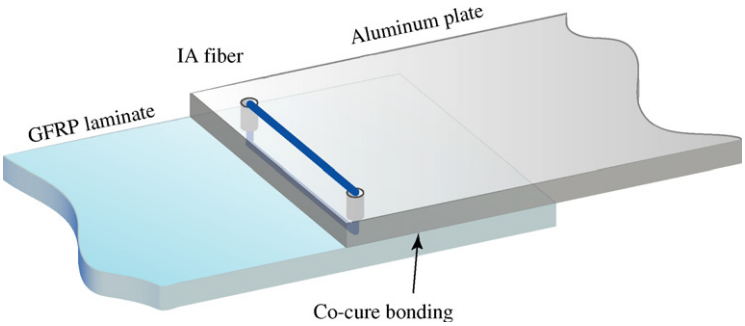

Fig. 1. Schematic illustration of the Inter-Adherend-Fiber joint between aluminum and GFRP laminate. The IA fiber penetrates into the GFRP and holes in the metal adherend, and unites both adherends with co-cure bonding.

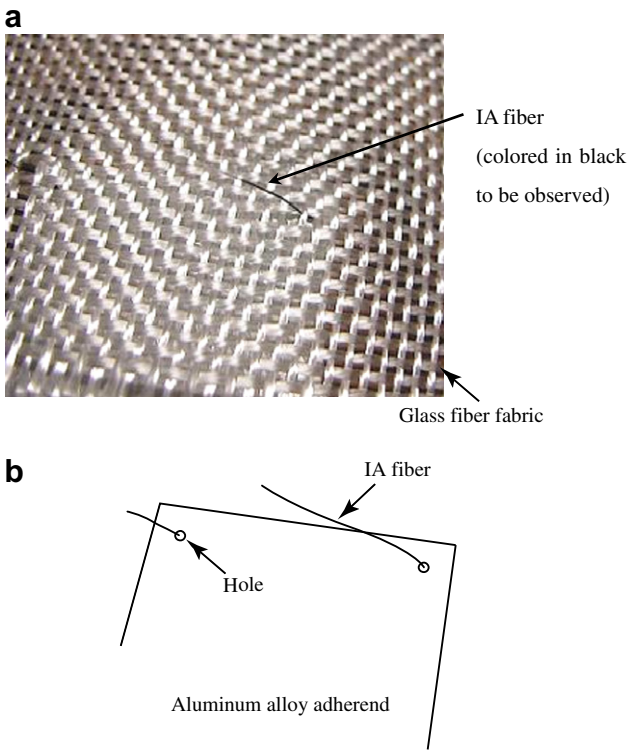

Fig. 2. Stacking process of the IAF joint using plain woven fabric GFRP. The IA fibers are inserted between the glass fiber warp and weft bundles without damaging fibers: (a) photograph; (b) illustration.

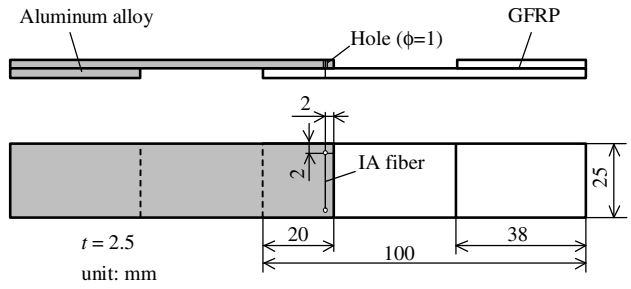

Fig. 3. Specimen configuration of the IAF joint between GFRP and aluminum.

IAF joint is shown in Fig. 3. Each adherend is 100 mm in length, 25 mm in width, 2.5 mm in thickness, and 20 mm in over-lap length; thus the over-lap area is about 500 mm^2. The glass fibers used are alkali-free plain-woven glass fabric YEM1801 (101.2 tex) produced by Solar Co. Ltd., while the matrix is two-component cold setting epoxy resin Z2/H07 by Kokusai Chemical Co. Ltd. The GFRP adherend is made from $[(0/90)_{12}]_T$ laminate(Young's modulus $E_1 = 13.0$ GPa). The 0 degree direction of the GFRP is along the longitudinal direction of the specimen; thus the 90-degree ply is in contact with the aluminum alloy surface. The metal adherend is aluminum–magnesium alloy A5052-F (Young's modulus 68.9 GPa). Glass fibers are brittle material and are easy to break due to penetrating process when the glass fibers are used as IA fibers. Thus, nylon fibers (diameter 0.165 mm, strength 19.6 N) produced by Asahi Kasei Corp., which are more ductile than glass fibers, are used as IA fibers.

Holes for the IAF in the metallic adherend are fabricated using a drilling machine with a diameter of 1 mm. A pair of holes are placed at 2 mm from the aluminum adherend edge as shown in Fig. 3. The surfaces of the aluminum alloy adherend are polished using P240 waterproof abrasive paper (JIS R 6253), and are wiped with acetone. The application of the proposed joints is small or mid-sized nautical vessels where Aluminum and GFRP are often used. Thus, a chemical treatment was not applied to the aluminum surface, being hardly feasible for large-scale marine structures.

Aluminum adherends are pre-cut prior to co-curing. The dry fabric glass fiber lamina is then stacked on the aluminum alloy adherend by hand lay-up. The IA fibers penetrate into the aluminum and glass fabric lamina adherends using a sewing needle. Multiple specimens are fabricated at the same time using continuous IA fiber as shown in Fig. 4. A certain tension force is applied to the IA fiber using a plummet at the edges of the IA fiber. Epoxy resin is then impregnated into the glass fabric. Then, 11 sheets of glass fiber fabric are laminated: the IA fiber is embedded as a line between first and second layers of GFRP. The specimens are cured at 25 °C for 24 h and 80 °C for 2 h at a pressure of 0.7 MPa in an electric furnace. The specimens are cut into the proper size using a diamond cutter. Fig. 5 shows a photograph of a typical fabricated IAF joint specimen.

To compare with the joining strength of conventional joints, co-cured aluminum/GFRP joints were also fabricated without IAF processing (non-IAF joints). The type and size of adherends are the same as for the IAF joint specimen.

3.2. Static tensile lap-shear tests

Static tensile lap-shear tests are carried out on the basis of JIS K 6850 using a tensile testing machine AG-I by Shimadzu Co., in order to evaluate the static strength of IAF joints. The experimental setup is illustrated in Fig. 6. The stroke speed is 1.0 mm/min. The strength is evaluated using the maximum tensile shear strength S, given by

$$S = \frac{P_{\max}}{A} \tag{1}$$

where $P_{\max}$ is the maximum applied load during the test and A is the adhesive area. The reduction in area due to the presence of the holes is not included in the calculation of the joint strength.

Acoustic emission (AE) measurements are also carried out to investigate the fracture mechanisms of the aluminum/GFRP co-cured joint with IAF during tensile loading tests. A 901S AE sensor and 9501 AE tester produced by NF Corp. are used for AE measurements. The AE event

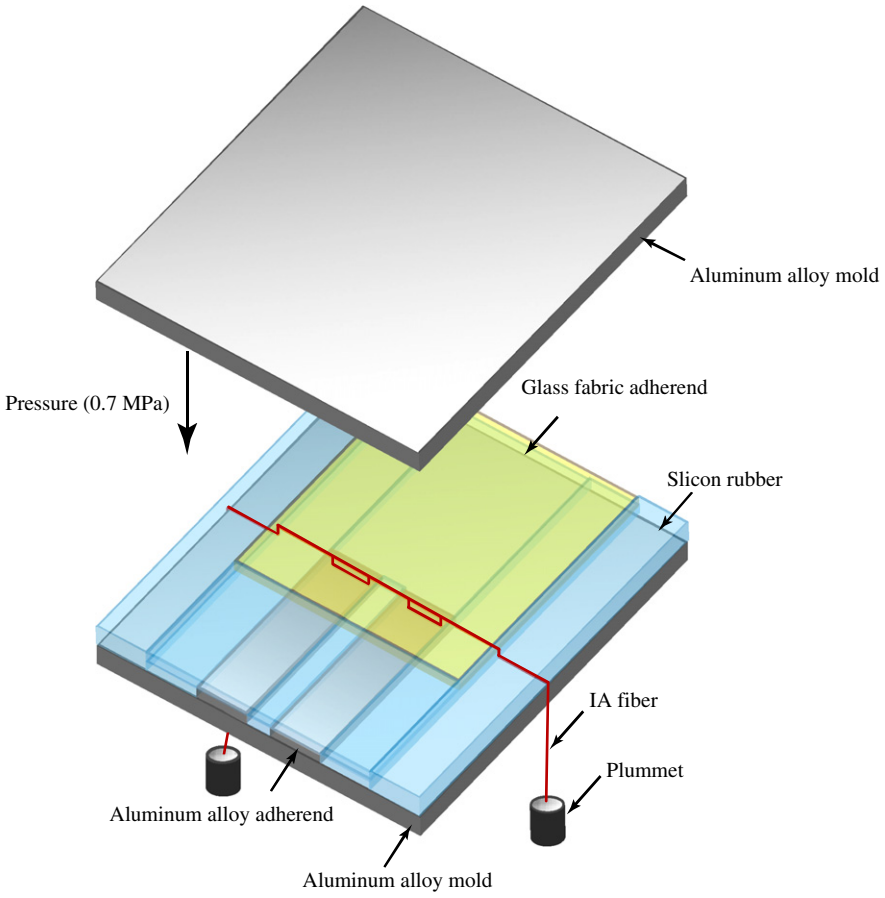

Fig. 4. Illustration of co-curing process of IAF joint specimens.

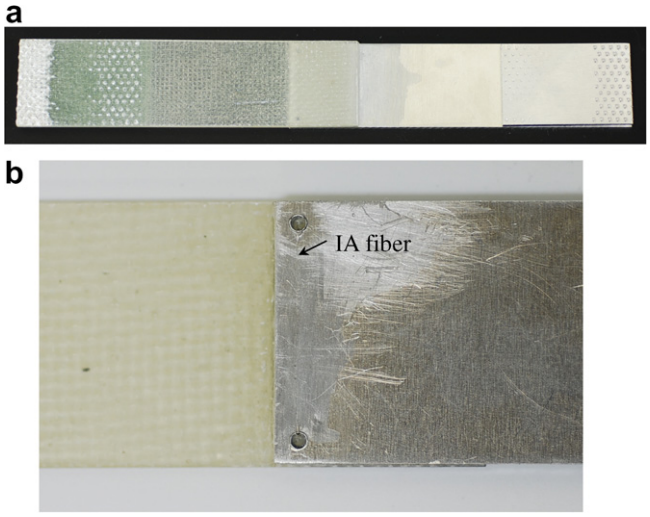

Fig. 5. Photograph of the aluminum/GFRP IAF joint specimen: (a) specimen overview (GFRP surface); (b) zoomed at the IAF (aluminum surface).

count rate is recorded using a PCD-320A sensor interface (Kyowa Corp.) and loaded into a PC.

The progressive crack fronts are observed by monitoring the GFRP surface during the tests using a digital video recorder. The observation uses the phenomenon that translucence of the GFRP adherend surfaces at the bonded area turns white due to an alteration in the refractive index when the crack occurs between the adherends.

3.3. Effect of IA fiber tension force

The joint strength with IAF may be affected by the mechanical properties and tension force of the IA fiber. The mechanical properties of IA fiber can be maintained constant by quality control of IA fibers; thereby the effect of the tension force on the joint strength is investigated by changing the weight of the plummet in the specimen production as 77 g, 100 g, 140 g, 170 g, and 200 g. The Z2/H07 resin is impregnated with the forced tension, and then the specimen is cured. Three IAF joint specimens at each tension force and five co-cured joint specimens without IAF are tested.

3.4. Tensile lap-shear fatigue tests

In the literature [14], no effect or a reduction in the fatigue life was observed in the stitched composites, even though they showed significant improvement in static

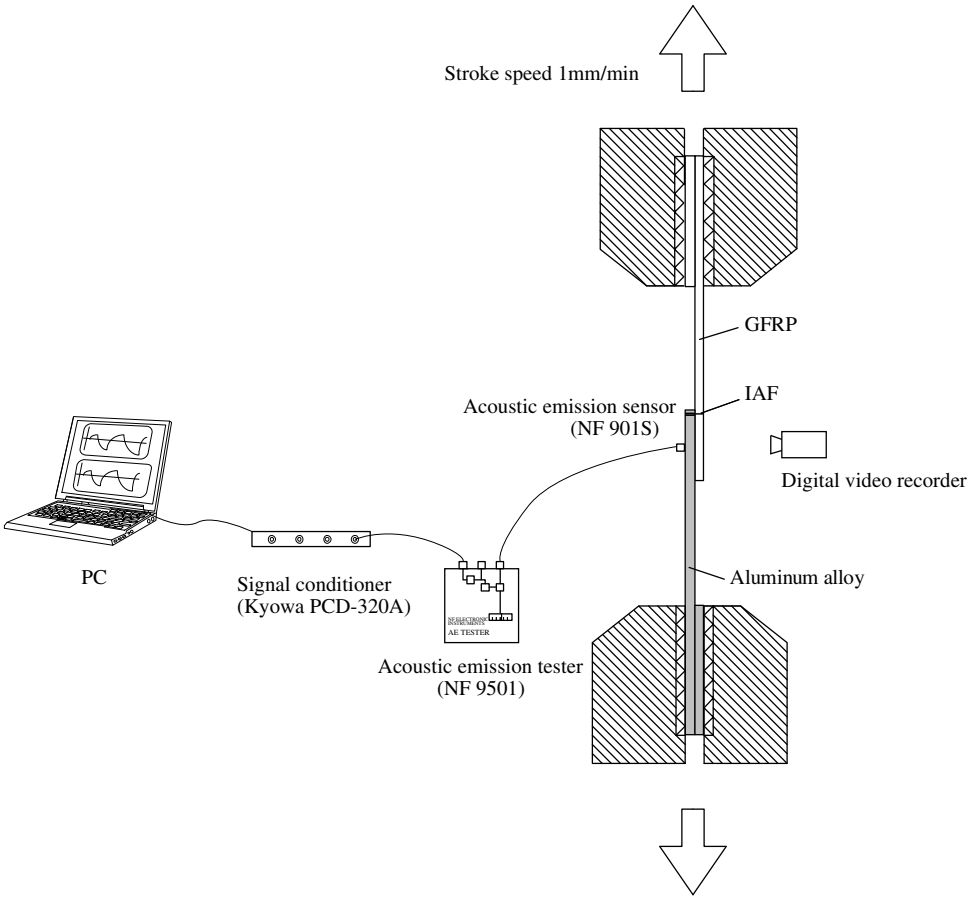

Fig. 6. Experimental setup of tensile lap-shear tests.

delamination resistance. Therefore, we examine the fatigue strength of the proposed IAF joints by conducting tensile lap-shear fatigue tests.

The fatigue tests are performed based on JIS K 6864: test methods for fatigue properties of structural adhesives in tensile shear using MTS servo material testing machine Model 312.21. Four IAF joints and five non-IAF joints were tested. The objective of the fatigue tests is to demonstrate failure trends of the IAF joints compared with a non-IAF joint rather than the generation of comprehensive *S-N* curves. The stroke is controlled as a sinusoidal wave and the frequency is from 10 Hz (IAF joint at the stress of 4.89 MPa) to 20 Hz (the other specimens); it was confirmed by means of measuring specimen temperature that the specimen does not generate excessive heat even at 20 Hz. The maximum shear stress τ_{max} and minimum stress τ_{min} are defined as maximum and minimum applied loads divided by the adhesive area, respectively; the stress ratio (τ_{min}/τ_{max}) is constant at 0.1 in all fatigue tests. The mean stress $\tau_m = (\tau_{max} + \tau_{min})/2$ is set to be in the range from 0.25 to 0.5 τ_R, where τ_R is the static tensile shear strength of each joint obtained in the static tests. Fatigue failure is defined here as the perfect separation between two adherends.

4. Results and discussion

4.1. Static tensile lap-shear tests

Fig. 7 shows the load–displacement curves of non-IAF and IAF co-cured joints. The zero tension force was applied to the IA fiber in the specimen fabrication. The abscissa is stroke displacement, and the ordinate is applied load. Figs. 8 and 9 show the AE measurement results for non-IAF and IAF joints, respectively. The ordinate is AE count rate and cumulative AE counts. The points A1 and A2 in Fig. 8 and B1–B4 in Fig. 9 correspond to the same numbers in Fig. 7. Fig. 10a–d are pictures of the GFRP adherend surface at the bonded area representing crack propagation observed using a digital video recorder during the tensile tests. The upper and lower lines correspond to the aluminum and GFRP adherend edges, respectively. The dashed lines are the front of the crack propagation predicted from the changing in the color of the GFRP surface.

As for the non-IAF co-cured joints, the applied load increases in proportional to the displacement until the point A1. From the recorded video image of the GFRP surface, the crack occurs from the aluminum edge at the point A1 and propagates toward the GFRP adherend edge.

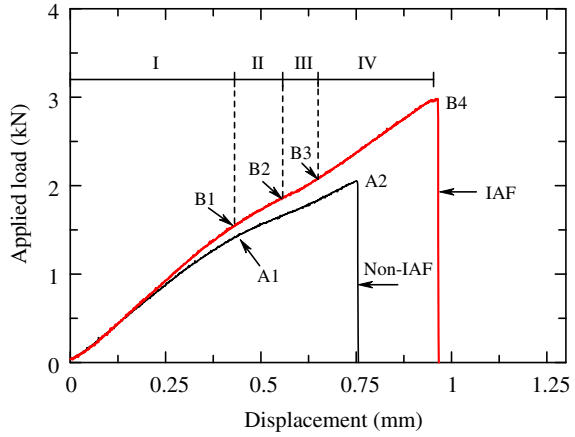

Fig. 7. Applied load and displacement diagram of aluminum/GFRP non-IAF and IAF joints. Adhesive crack and adhesive joint failure occur at A1 and A2 in the non-IAF joint, respectively. For the IAF joint, a crack occurs at the aluminum edge at B1; and propagates to the position of the IAF; the crack propagation stops at B2 until B3; another crack occurs at the GFRP edge at B3 and progresses to the aluminum edge; and finally the IAF joint breaks at B4.

AE measurements also show the large AE at the point A1 in Fig. 8. The occurrence of an adhesive crack decreases the joint stiffness after A1. A large number of AEs are observed, and the gradient of cumulative AE counts increases until the joint breaks at A2, at a displacement of 0.75 mm. The failure mode of non-IAF joints is a mixture of the adhesive failure and a small amount of GFRP adherend failure.

As for the IAF joints, considering the load–displacement curve, AE measurements and visual observation, the failure mechanisms are divided into four phases:

Phase(*I*) Elastic deformation (until B1)The applied load to the IAF joint increases in proportion to the displacement until the point B1. Since the apparent crack does not form in this phase, few AEs are observed. The stiffness is approximately the same as for the non-IAF joints.

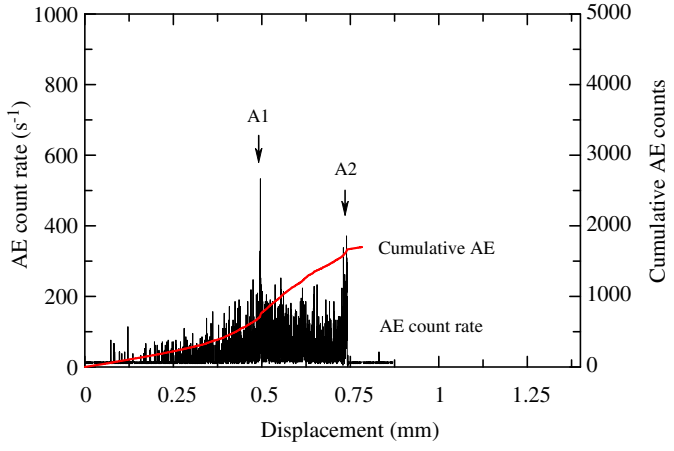

Fig. 8. Acoustic emission (AE) count rate and cumulative AE counts for non-IAF joints during static tensile–shear tests. A1 and A2 correspond to the same numbers in Fig. 7.

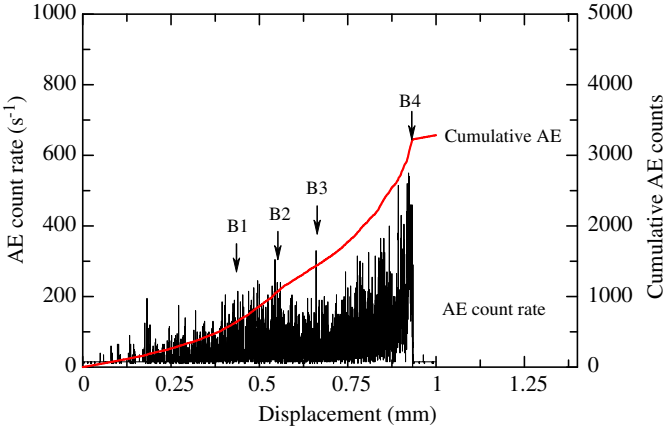

Fig. 9. Acoustic emission (AE) count rate and cumulative AE counts for IAF joints during static tensile–shear tests. B1, B2, B3 and B4 correspond to the same numbers in Fig. 7.

Phase(*II*) Crack formation at the aluminum edge (from B1 to B2)A crack forms at the edge of the aluminum adherend edge at B1. The initial crack formation is not as apparent as for non-IAF joints. This is because small cracks form gradually due to the presence of defects including fiber waves and resin richness from the IAF penetration. The displacement to the initial crack is approximately the same as for the non-IAF joints. This indicates that the IAF is not efficient in delaying the initial crack formation. The crack at the aluminum edge propagates to the edge of the GFRP direction, thereby a large number of AEs are observed in this phase, and the gradient of cumulative AE counts increases as shown in Fig. 9. The stiffness of the IAF joints decreases a little due to partial debonding of the two adherends.

Phase(*III*) Cessation of crack propagation (from B2 to B3)The propagation of the crack stops at the IAF point due to the presence of the IA fiber. The stopped crack is observed in the picture shown in Fig. 10b. Since the crack progress is prevented in this phase, the gradient of cumulative AE counts decreases (B2).

Phase(*IV*) Crack formation at the GFRP edge (from B3 to B4)Another crack occurs at the GFRP edges and travels toward to the aluminum edges. The AE count rate increases again. While the crack propagates from the GFRP edge to the aluminum edge, the crack that previously formed at the aluminum edge still stops at the IAF point as shown by the side view of the joints in Fig. 11. This is clearly observed in Fig. 10c. When the crack from the GFRP edge propagates to the IAF point, all of the lap area is debonded as shown in Fig. 10d; the joint finally breaks.

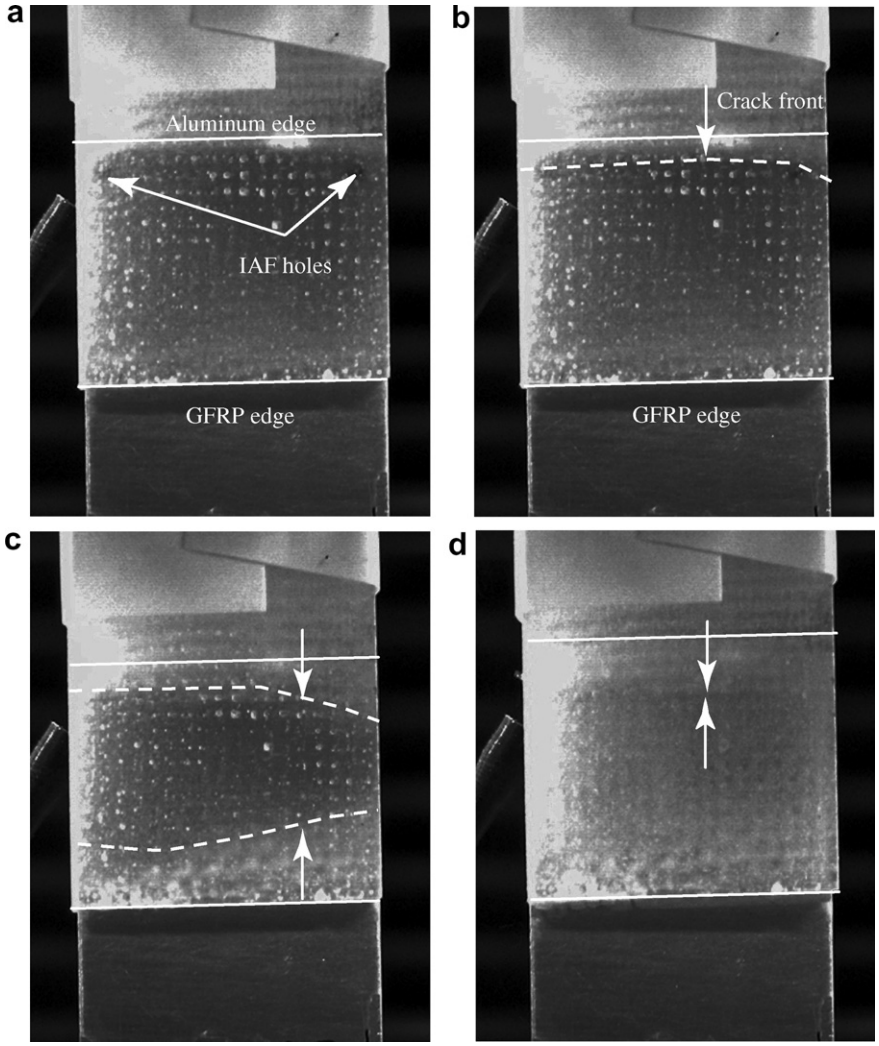

Fig. 10. Crack propagation of the IA joint during tensile shear tests: (a) *Phase I*; (b) *Phases II* and *III*; (c) *Phase IV*; (d) the adhesive joint failure at B4. The solid line indicates the edges of aluminum and GFRP adherends; the dashed lines are the crack fronts.

Fig. 12 shows the failure surfaces of the aluminum and GFRP adherends. The pulled IA fibers, epoxy resin and a small amount of glass fibers are observed on the aluminum adherends. The pullout of the IA fiber from the GFRP adherend occurs just before the joint failure, which corresponds to the maximum point in the load–displacement curves in Fig. 7. Thereby, the IA fiber performs as a bridge between the two adherends after the adhesive failure until the joint failure. The failure mode of the IAF joints is a mixture of adhesive failure and a small amount of GFRP adherend failure followed by the IAF fiber failure. Although the stiffness is not much different between IAF and non-IAF joints, the displacement to failure increases about 27% using IAF. This increases the strength of IAF lap joints compared with non-IAF joints. The IA fibers at the both sides may increase the final

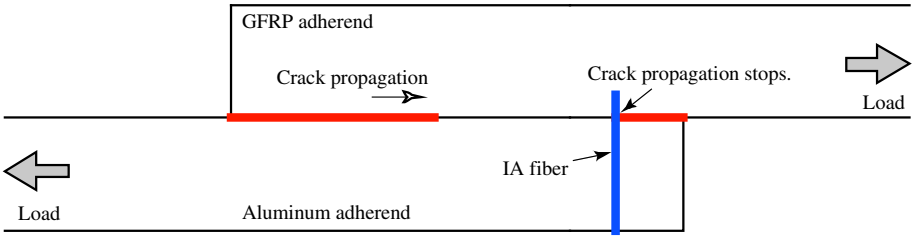

Fig. 11. Side view of the IAF joint in *Phase IV*: the crack previously formed at the aluminum edge stops at the IAF point while another crack propagates from the GFRP edge.

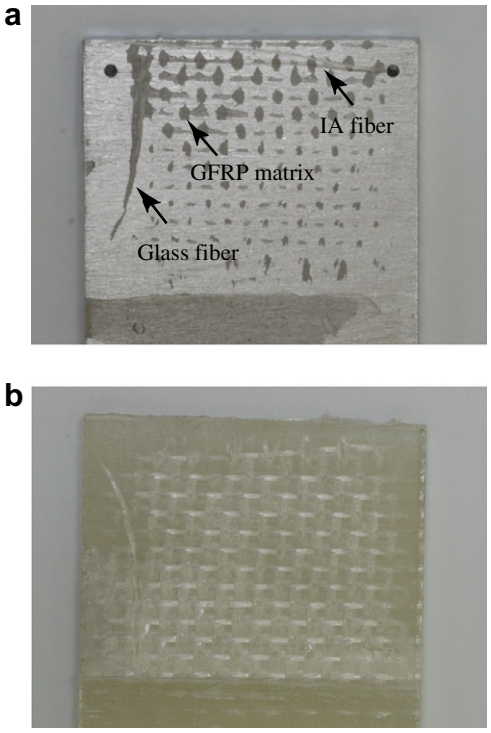

Fig. 12. Failure surfaces of the aluminum/GFRP IAF joint after static tensile shear tests: (a) aluminum adherend; (b) GFRP adherend.

strength. The proper IA fiber locations will be investigated in the future.

Fig. 13 shows the average tensile shear lap joint strength of the IAF joints compared with non-IAF joints. The average joint strengths are 5.47 MPa for non-IAF joints and 6.32 MPa for IAF joints; thus the IAF treatment increases the joint strength about 15%. The error band indicates the maximum and minimum data; the scatters are approximately the same for the non-IAF and IAF joints. The scatter in IAF joints is mainly due to the zero tension force of the IA fiber: the zero tension force causes a wide quantity variation in the resin rich area at adhesive interface especially around the IA fiber. In the IAF joints, a high proportion of the tensile load is applied to the IA fiber and around the fiber when the IAF joints breaks. Thus, the strength of the IAF joints highly depends on the IAF condition. On the other hand, the non-IAF joints break mainly by adhesive failure; the strength depends much more on the surface condition than is the case for the IAF joints. Thereby, the scatter in the non-IAF joints is due to surface condition variation including roughness and purity.

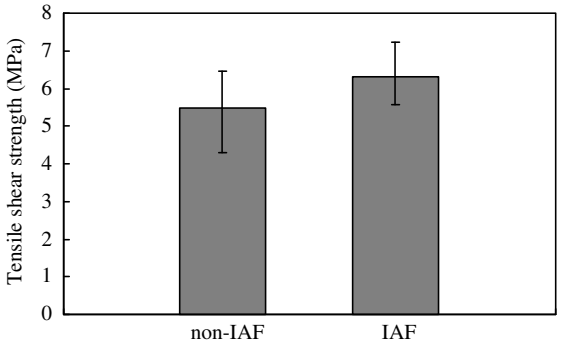

Fig. 13. Average static tensile shear strengths of aluminum/GFRP non-IAF and IAF joints.

4.2. Effect of the tension force

Fig. 14 shows the load–displacement curves of IAF joints of 0.75 N, 1.37 N and 1.67 N tension forces of the IA fiber. Fig. 15 shows the average tensile shear strength of IAF joints varying the tension force of IA fibers. The ordinate is the tensile shear strength and the abscissa is the tension force of the IA fiber. A zero tension force corresponds to the results in Fig. 13. The results for non-IAF joints are also depicted, as open circles. The IA fiber breaks during material processing in the case of the heaviest plummet of 200 g (1.96 N), which makes it impossible to perform the tensile experiment. Although the applied tension force of 1.96 N is much lower than the fiber strength of 19.6 N given by the manufacturer, the applied tension force

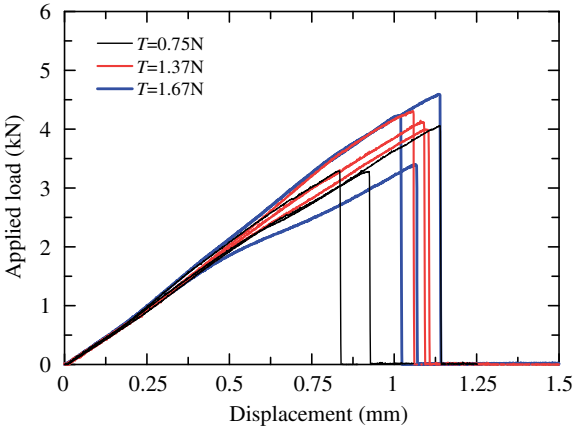

Fig. 14. Load–displacement curves of the IAF joint varying the tension force of the IA fiber: 0.75 N, 1.37 N, and 1.67 N.

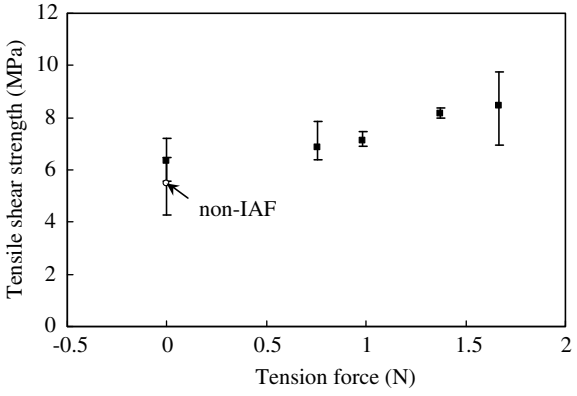

Fig. 15. Effect of tension force of the IA fiber on the tensile shear strength of IAF joints: IAF joint (square symbol); non-IAF joint (circle symbol).

to the fiber is concentrated at the edge of the specimen, and the maximum applied force may be beyond the tension strength of the IA fibers.

As can be seen from Fig. 15, the tensile shear strength increases and its scatter decreases with increasing tension force. This is because the warping of the IA fiber is suppressed, and glass fiber bundles firmly contact the aluminum surface. This decreases the resin rich area, and induces mechanical locking between GFRP and aluminum adherend. This results in increasing the peeling resistance. The decrease in the resin richness could also attribute to the decrease in the strength scatter. The scatter of the tensile shear strength has a minimum at a tension force of 1.37 N, whereas the tension force of 1.67 N has a large scatter of the tensile shear strength. This is because the excess high-tension force warps the glass fiber alignment locally, and increases defects including fiber damage and local resin richness. From these results, the optimum tension force 1.37 N of the IA fiber realizes high strength and low scatter in the IAF joints.

4.3. Tensile lap-shear fatigue tests

The failure mode of the IAF joints is a mixture of IAF fiber breaking, adhesive failure and GFRP adherend failure. The crack propagation is similar to that of the static results: a crack occurs at the aluminum adherend edge and is prevented at the IAF point; then another crack starts from the GFRP adherend edge; finally the adhesive joint failure occurs.

Fig. 16 shows the *S-N* curves of the fatigue tests using IAF and non-IAF joints. The abscissa is the logarithmic of the number of cycles, while the ordinate is the maximum stress τ_{max}. Although comprehensive *S-N* curves are not obtained, it can be said that the IAF joints have similar fatigue strength to that of the non-IAF joints. The reason why IAF is less effective in prolonging the fatigue life is that the IA fibers are prone to damage under fatigue loading.

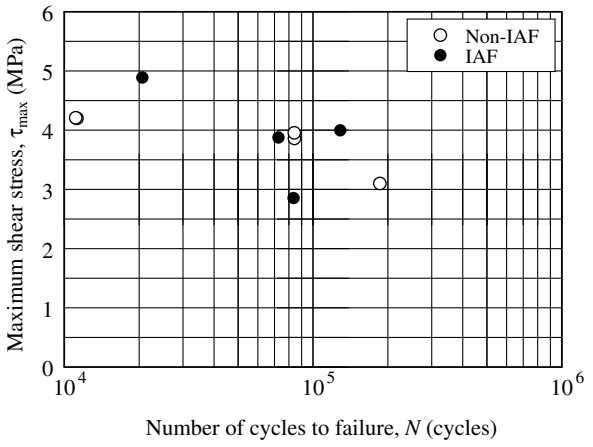

Fig. 16. Maximum shear stress and number of cycles to failure for the aluminum/GFRP non-IAF joint (open circles) and IAF joints (solid circles). The stress ratio R is 0.1.

However, since the IAF treatment does not have adverse affects on the fatigue properties, we conclude that the IAF joints have proven to be effective in realizing high static strength and low strength scatter without decreasing the fatigue performance. For long-term use, proper protection such as resin coating on the IA fiber will be needed since the IA fibers are exposed to external environment.

5. Conclusions

The present study experimentally investigated an improvement in the strength of metal/composite co-cured joints using IA fibers. The static and fatigue tensile–shear tests of IAF joints were compared with those for non-IAF joints. The experiments demonstrate the IA fiber performs as a bridge between the metal and composite adherends; it reduces the driving force of the crack propagation at the crack tip, and efficiently arrests the propagation. As a consequence, the displacement to failure and ultimate static strength are significantly increased using IAF without a decrease in the fatigue strength. It was also revealed that the IA fiber with an optimum tension force realizes a metal/composite co-cured joint having high static strength with low scatter.

References

[1] Kim HS, Lee SJ, Lee DG. Development of a strength model for the cocured stepped lap joints under tensile loading. Compos Struct 1995;32:593–600.
[2] Huang CK. Study on co-cured composite panels with blade-shaped stiffeners. Composites: Part A 2003;34:403–10.
[3] Shin KC, Lim JO, Lee JJ. The manufacturing process of co-cured single and doublelap joints and evaluation of the load-bearing capacities of co-cured joints. J Mater Process Technol 2003;138:89–96.
[4] Kim HS, Park SW, Lee DG. Smart cure cycle with cooling and reheating for co-cure bonded steel/carbon epoxy composite hybrid structures for reducing thermal residual stress. Composites: Part A 2006;37:1708–21.
[5] Olivier P, Cottu JP. Optimization of the co-curing of two different composites with the aim of minimising residual curing stress levels. Compos Sci Technol 1998;58:645–51.
[6] Park SW, Kim HS, Lee DG. Optimum design of the co-cured double lap joint composed of aluminum and carbon epoxy composite. Compos Struct 2006;75:289–97.
[7] Shin KC, Lee JJ. Effects of thermal residual stresses on failure of co-cured lap joints with steel and carbon fiber-epoxy composite adherends under static and fatigue tensile loads. Composites: Part A 2006;37:476–87.
[8] Sankar BV, Sharma SK. Mode II delamination toughness of stitched graphite/epoxy textile composites. Compos Sci Technol 1997;57:729–37.
[9] Jain LK, Dransfield KA, Mai Y-W. On the effects of stitching in CFRPs – II. Mode II delamination toughness. Compos Sci Technol 1997;58:829–37.
[10] Dransfield KA, Jain LK, Mai Y-W. On the effects of stitching in CFRPs – I. Mode I delamination toughness. Compos Sci Technol 1997;58:815–27.
[11] Gunnion AJ, Scott ML, Thomson RS, Hachenberg D. Thickness effects on the compressive stiffness and strength of stitched composite laminates. Compos Struct 2004;66:479–86.

[12] Chen G, Li Z, Kou C, Gui L. Finite element analysis of low-velocity impact damage of stitched laminates. J Reinf Plast Compos 2004;23(9):987–95.
[13] Byun J-H, Song S-W, Lee C-H, Um M-K, Hwang B-S. Impact properties of laminated composites with stitching fibers. Compos Struct 2006;76:21–7.
[14] Aymerich F, Priolo P, Sun CT. Static and fatigue behaviour of stitched graphite/epoxy composite laminates. Compos Sci Technol 2003;63:907–17.
[15] Mouritz AP. Ballistic impact and explosive blast resistance of stitched composites. Composites: Part B 2004;32:431–9.
[16] Tong L, Steven GP. A numerical study on stresses in resin transfer moulding lap joints reinforced with transverse stitching. Compos Struct 1996;36:91–100.
[17] Tong L, Jain LK, Leong KH, Kelly D, Herszberg I. Failure of transversely stitched RTM lap joints. Compos Sci Technol 1997;58:221–7.
[18] Aymerich F, Onnis R, Priolo P. Analysis of the fracture behaviour of a stitched single-lap joint. Composites: Part A 2005;36:603–14.
[19] Aymerich F, Onnis R, Priolo P. Analysis of the effect of stitching on the fatigue strength of single-lap composite joints. Compos Sci Technol 2006;66:166–75.
[20] Byrd LW, Birman V. Effectiveness of z-pins in preventing delamination of co-cured composite joints on the example of a double cantilever test. Composites: Part B 2006;37:365–78.
[21] Dantuluri V, Maiti S, Geubelle PH, Patel R, Kilic H. Cohesive modeling of delamination in Z-pin reinforced composite laminates. Compos Sci Technol 2007;67:616–31.
[22] Chang P, Mourtiz AP, Cox BN. Properties and failure mechanisms of pinned composite lap joints in monotonic and cyclic tension. Compos Sci Technol 2006;66:2163–76.
[23] Chang P, Mouritz AP, Cox BN. Flexural properties of z-pinned laminates. Composites: Part A 2007;38:244–51.
[24] Melograna JD, Grenestedt JL. Improving joints between composites and steel using perforations. Composites: Part A 2002;33:1253–61.
[25] Melograna JD, Grenestedt JL, Maroun WJ. Adhesive tongue-and-groove joints between thin carbon fiber laminates and steel. Composites: Part A 2003;34:119–24.
[26] Matsuzaki R, Shibata M, Todoroki A. Evaluation of dimple treatment for GFRP/metal co-cured joint. Key Eng Mater 2006;324–325:1729–32.
[27] Matsuzaki R, Shibata M, Todoroki A. Improving performance of GFRP/aluminum single lap joints using bolted/co-cured hybrid method. Composites: Part A 2008;39:154–63.